Optical and microstructural characterization of sol–gel derived cerium-doped PZT thin films

S. B. MAJUMDER, Y. N. MOHAPATRA, D. C. AGRAWAL
Materials Science Programme, IIT Kanpur 208016, India

Optical properties of cerium-doped PZT thin films on sapphire prepared by a sol–gel technique are investigated using both transmission and reflection spectra in the wavelength range 200 to 900 nm. The refractive index, extinction coefficient and thickness of the film are determined from the measured transmission spectra. The packing density of the film is calculated from its refractive index using the effective medium approximation (EMA), and average oscillator strength and wavelength are estimated using a Sellmeir-type dispersion equation. Absorption coefficient (α) and the band gap energy (E_g) of each film composition are also calculated. Possible correlations of microstructure and phase formation behaviour with changes in band gap energy and other optical properties are discussed.

1. Introduction

Thin ferroelectric films are at present being studied intensively due to their proposed uses in various fields. Materials under active consideration include lead zirconate titanate (PZT), lead titanate (PT) and lanthanum-doped PZT (PLZT). These compounds have a unique blend of properties such as ferroelectricity, piezoelectricity and electro-optic phenomena [1]. Thin films of these materials have been successfully employed in the fabrication of non-volatile memories [2], surface acoustic wave (SAW) devices, delay lines [3], infrared (IR) optical field effect transistors [4] and electro-optic switches and modulators [5]. For successful device application the films should be characterized in terms of their phase formation behaviour, microstructure and ferroelectric properties [6–9].

Very limited reports exist on the optical characterization of PZT thin films. The optical characterization gives valuable insight into the structural parameters of the thin film such as packing fraction (f), thickness (d_f) and surface roughness (indicated qualitatively by the extinction coefficient (k)) [10]. The properties of the films can be modified by the addition of small amounts of dopants which replace one or more host atom(s) in the PZT lattice. In general dopants can be of two different types: donors (having valency higher than the host atoms they replace) and acceptors (having valency lower than the host atom). To maintain the electrical neutrality vacancies are produced and the presence of these vacant lattice sites modifies the properties [1].

Limited reports exist on the structure–property relationship of doped PZT thin films. A few reports are available on acceptor-doped PZT [11, 12] and donor-doped PZT thin films [13, 14] but there are hardly any reports on the effect of isovalent substitution. Ce^{4+} has large solid solubility in ZrO_2 [15]. In the present work we have studied Ce^{4+}-doped PZT films. Ce^{4+} is expected to occupy the B (Zr^{4+}, Ti^{4+}) sites and act as an isovalent dopant. The ionic radii of Ce^{4+} (atomic radius, $r = 0.094$ nm, coordination number (CN) = 6) and Zr^{4+} ($r = 0.086$ nm, CN = 6) are the same to within 15%. In the present work the phase formation behaviour, surface morphology and optical properties of the Ce-doped thin films have been studied and possible correlations have been discussed.

2. Experimental details

2.1. Preparation of precursor sol for coating

$Pb(Zr_{0.535-\delta}Ce_{\delta}Ti_{0.465})O_3$ thin films were prepared on sapphire $(1 1 \bar{2} 0)$ substrates by a sol–gel route. The mole concentrations (δ) of Ce were taken to be 0 (undoped), 0.05, 0.1 1, 3, 5 and 10. Pb-acetate was dissolved in glacial acetic acid and heated to 110 °C in a three neck flask condenser assembly to remove the associated water of crystallization. Zr-4-propoxide and Ti-4 -butoxide were also co-mixed in the required amounts. Glacial acetic acid was added to this mixture and stirred for 15 min. A calculated amount of $Ce(NO)_3 \cdot 6H_2O$ was separately dissolved in isopropanol and after dissolution it was added dropwise to the Zr–Ti sol with continuous stirring. The complex Ce–Zr–Ti sol thus produced was added to Pb-acetate solution at 90 °C with continuous stirring for about 20 min and stored in an airtight polypropylene container. The complex PZT–Ce sol thus prepared is termed as the parent sol. The amounts of chemicals used are summarized in Table I. For the coating, the parent sol was diluted to $0.3\ \mathrm{M\,L^{-1}}$ with the isopropanol and the acetic acid mixture.

0022–2461 © 1997 Chapman & Hall

TABLE I Composition of the precursor sol

	(moles)
Lead acetate trihydrate	1.05
Zirconium-4-propoxide	$(0.535 - \delta)$ $\delta = 0$, 0.0005, 0.001, 0.01 0.03, 0.05 and 0.1
Cerium nitrate hexahydrate	δ
Ti-4-butoxide	0.465
Glacial acetic acid	6
Isopropanol	1.25

2.2. Deposition and heat treatment of the films

Sapphire single crystals were cleaned thoroughly in a series of organic solvents by ultrasonication and finally with absolute alcohol. The diluted sol was spun coated on cleaned sapphire at 5000 r.p.m. for 20 s. Just after deposition the film was directly inserted in a preheated furnace at 400 °C and heated for 20 min in flowing oxygen to remove organics, and then quenched in ambient air. The film was recoated and reheat-treated 10 times, as above, to increase the film thickness. After the last coating, the furnace temperature was increased at a rate of 8–10 °C min^{-1} up to 700 °C, held for 1 h and then cooled down to room temperature.

2.3. Phase evaluation

The phases in the films were evaluated using a X-ray diffractometer (Rich Seifert Iso-Debyeflex 2002) with Ni-filtered CuK_α radiation. It was found that for all compositions only a rhombohedral phase was present. Lattice parameters a_R and α_R of the rhombohedral phase were determined using the (2 0 0) and (1 0 2) peaks following a procedure employing hexagonal conversion [16].

2.4. Surface morphology

The surface morphology of the film was studied in a scanning electron microscope (SEM) (JSM 840A Jeol Corporation) after coating the film with a thin layer of Au–Pd. The grain size distribution of the film was measured using a semi-automated image analyser (Leitz ASM 68K).

2.5. Optical transmission and reflection spectra measurement

The transmission and reflection spectra were recorded by a UV–VIS scanning spectrophotometer with integrating sphere arrangement (Hitachi 150-20). The transmission spectra of the samples were measured using air as reference. The reflectance spectra of the samples were recorded with respect to a standard sample having 100% reflectance. During the measurements the range of wavelength scanned was 200–900 nm at scanning rate 200 nm min^{-1} and sampling interval of 5 nm.

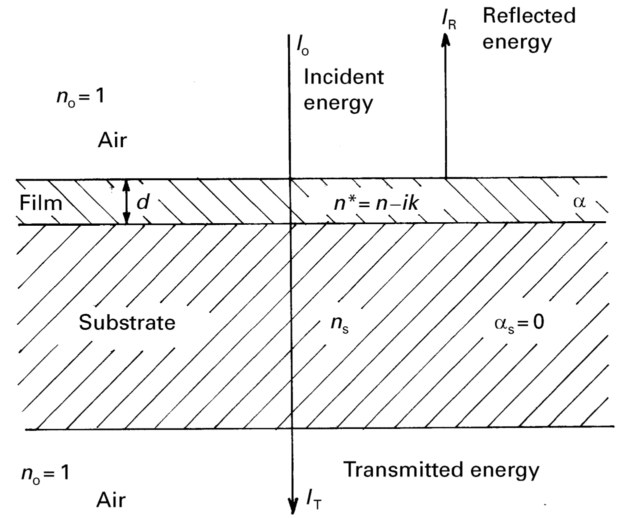

Figure 1 Reflection and transmission of light by a single film deposited on a weakly absorbing transparent substrate.

3. Optical constants evaluation

In the present work the optical constants were evaluated using the "envelope method" originally developed by Manifacier *et al.* [17]. For an insulating film on a transparent substrate (Fig. 1), if we assume that (i) the film is weakly absorbing and (ii) the substrate is completely transparent, then using this method the refractive index (n), extinction coefficient (k), the film thickness (d) and the absorption coefficient (α) of the film can be evaluated from the transmission spectra as summarized below.

When

$$k^2 \ll (n - n_0)^2$$

(n_0 refractive index of air)

and

$$k^2 \ll (n - n_s)^2$$

(n_s refractive index of substrate)

then the transmittance (T) of the film can be described as

$$T = \frac{(16 n^2 n_0 n_s x)}{C_1^2 + C_2^2 \exp(-8\pi k d/\lambda) - 2 C_1 C_2 x \cos(4\pi n d/\lambda)} \tag{1}$$

where,

$$x = \exp(-4\pi k d/\lambda)$$

$$C_1 = [(n + n_0)(n_s + n)]$$

$$C_2 = [(n - n_0)(n - n_s)]$$

The film absorption coefficient, α, is related to k and wavelength, λ,

$$\alpha = 4\pi k/\lambda \tag{2}$$

The cosine in the denominator of Equation 1 oscillates between $+1$ and -1 so that

$$T_{\max} = 16 n_0 n_s n^2 x/(C_1 - C_2 x)^2 \tag{3}$$

$$T_{\min} = 16 n_0 n_s n^2 x/(C_1 + C_2 x)^2 \tag{4}$$

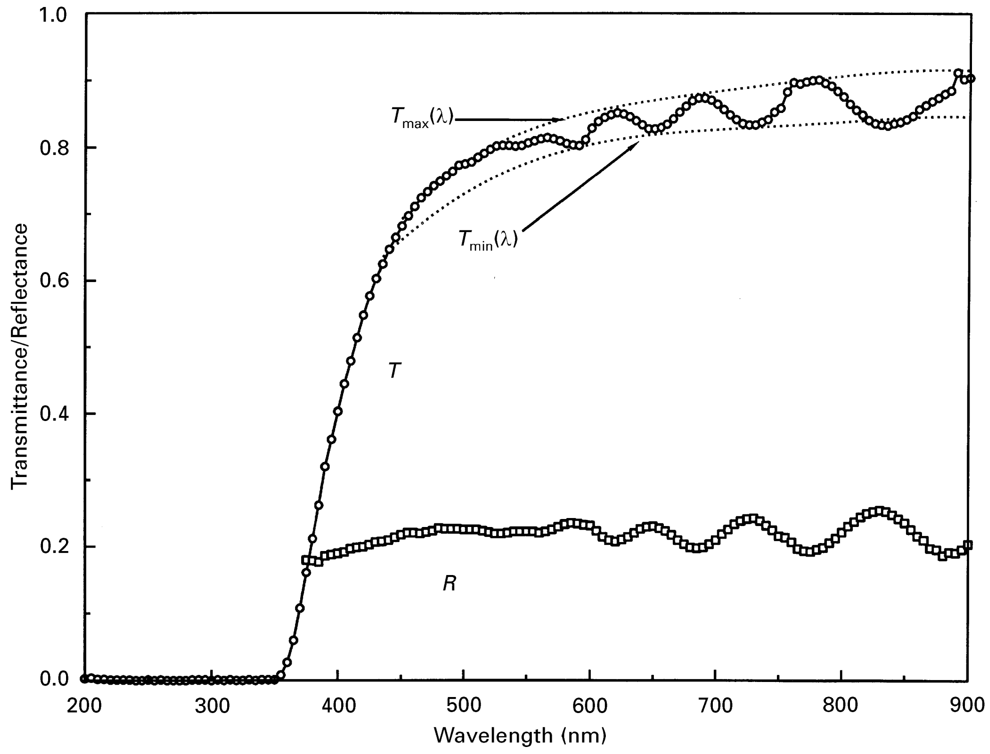

Figure 2 Transmittance and reflectance spectra and the T_{max} and T_{min} envelopes for undoped PZT film.

Light waves from air–film and film–substrate interfaces interfere giving rise to interference fringes. A satisfactory free-hand envelope curve is drawn through the maxima and minima points of the interference fringes. Then the graph is digitized and polynomial best fits $T_{max}(\lambda)$ and $T_{min}(\lambda)$ are obtained. In other words the transmittance spectrum is enveloped by $T_{max}(\lambda)$ and $T_{min}(\lambda)$ best fitted curves. Fig. 2 shows the % T, % R spectra along with the best fitted $T_{max}(\lambda)$ and $T_{min}(\lambda)$ curves.

Now from Equations 3 and 4 one can solve,

$$x = \exp(-\alpha d) \tag{5}$$

$$= \frac{(n+1)(n+n_s)[(T_{max}/T_{min})^{0.5} - 1]}{(n-1)(n-n_s)[(T_{max}/T_{min})^{0.5} + 1]} \tag{6}$$

and

$$n = [N' + (N'^2 - n_s^2)^{0.5}]^{0.5} \tag{7}$$

where

$$N' = \tfrac{1}{2}(1 + n_s^2) + \frac{2n_s(T_{max} - T_{min})}{(T_{max}T_{min})}$$

The refractive index (n_s) of the sapphire substrate as a function of photon wavelength (λ) can be calculated using the following dispersion relation [18]

$$n_s^2 = 1 + \frac{A\lambda^2}{\lambda^2 - \lambda_1^2} + \frac{B\lambda^2}{\lambda^2 - \lambda_2^2} + \frac{C\lambda^2}{\lambda^2 - \lambda_3^2} \tag{8}$$

where $A = 1.023\,798$, $B = 1.058264$, $C = 5.280\,792$, $\lambda_1 = 0.003\,775\,88$, $\lambda_2 = 0.012\,2544$, $\lambda_3 = 321.3616$, and λ is in μm.

3.1. Evaluation of the refractive index (n) of the film

The refractive index (n) of the film as a function of the incident photon wavelength (λ) was calculated using Equation 7. The data $n(\lambda)$ can be fitted to a Sellmeir-type dispersion relation [19]. For pure material the wavelength dependence of optical constants was treated by Lorentz [20]. The theory assumes that the material is composed of a series of independent oscillators which are set to forced vibrations by the incident radiation. For semiconducting and insulting materials the single term Sellmeir dispersion formula for one dominant electronic oscillator is [19]

$$n^2(\lambda) - 1 = \frac{S_0\lambda_0^2}{1 - (\lambda_0/\lambda)^2} \tag{9}$$

where S_0 is an average oscillator strength and λ_0 is an average oscillator wavelength, obtained from the slope and infinite wavelength intercept of the extrapolated straight line of $(n^2(\lambda) - 1)^{-1}$ versus $1/\lambda^2$ plot.

3.2. Determination of the film thickness

The thickness (d) of the film was calculated using the following relation [10]

$$d' = \frac{\lambda_1\lambda_2}{2[n(\lambda_1)\lambda_2 - n(\lambda_2)\lambda_1]} \tag{10}$$

where $n(\lambda_1)$ and $n(\lambda_2)$ are the refractive indices at two adjacent maxima (or minima) at λ_1 and λ_2. A number of d' values are thus obtained. Their average $(\bar{d})'$ is calculated. Now the well known formula for interference fringes is

$$2n\bar{d}' = m'\lambda \tag{11}$$

Here m' is an integer for maxima and a half integer for minima. Using $(\bar{d})'$, m' is obtained from Equation 11. It is rounded off to the nearest integer for maxima or half integer for minima to get the modified m. Now again from Equation 11 using these m, λ and n, a set of accurate d is obtained. The thickness of the film is the average of d, i.e. $\bar{d}$.

3.3. Evaluation of the absorption coefficient (α) and extinction coefficient (k)

Knowing x from Equation 6 and the thickness (d) as described above, we have calculated α from Equation 5 and k from Equation 2.

3.4. Calculation of optical constants near optical band-gap

Near the absorption edge, the refractive index can be calculated using the following relation [10]:

$$n = \frac{(1 + R^{0.5})}{(1 - R^{0.5})} \tag{12}$$

The transmittance value here is less than 40%. The absorption coefficient (α) has been calculated from the following relation [10].

$$\alpha = \frac{1}{d} \ln \left[\frac{(1 - R)\left\{1 - \frac{(n - n_s)^2}{(n + n_s)^2}\right\}\left\{1 - \frac{(n_s - 1)^2}{(n_s + 1)^2}\right\}}{T} \right] \tag{13}$$

where R and T are the reflectance and transmittance at a particular wavelength, n and n_s are the refractive indices of film and substrate, respectively, and d is the film thickness.

For a direct band gap material the absorption coefficient as a function of photon energy can be expressed as [21]

$$\alpha^2 = \text{Constant}(hc/\lambda - E_g) \tag{14}$$

where α is the absorption coefficient, (hc/λ) is the incident photon energy and E_g is the band gap energy.

By plotting α^2 versus (hc/λ), E_g can be evaluated from the extrapolated linear portion of the plot.

3.5. Evaluation of packing fraction

In a heterogeneous medium the effective dielectric constant is related to the dielectric constant of each component according to the effective medium approximation (EMA) as described by Bruggeman [22]

$$\sum_{i=1}^{n} f_i \frac{\varepsilon_i - \varepsilon}{\varepsilon_i + 2\varepsilon} = 0 \tag{15}$$

where ε_i and f_i are the dielectric constant and volume fraction, respectively, of the ith component and ε is the effective dielectric constant. However for most insulating films the extinction coefficient (k) is much smaller than the refractive index (n) and the dielectric constant (ε) is related to the refractive index by the following relation

$$\varepsilon = n^2 \tag{16}$$

In the present case the film is assumed to be a single phase material containing some amount of porosity. Hence

$$f \frac{n_b^2 - n^2}{n_b^2 + 2n^2} + (1 - f) \frac{(1 - n^2)}{(1 + 2n^2)} = 0 \tag{17}$$

where n_b is the refractive index of bulk PZT having Zr/Ti ratio 0.53/0.47 and f is the fractional porosity. The value of n_b at this composition could not be found in the literature. Thatcher [23] reported n_b for lead zirconate (PZ) and lead titanate (PT) as 2.420 and 2.668, respectively, at $\lambda = 632.8$ nm. We have interpolated these two data points to obtain $n_b = 2.55$.

4. Results and discussion

4.1. Phase analysis

All the films used for optical measurements had perovskite structure. Fig. 3 shows the X-ray diffractograms of undoped and Ce-doped films. The undoped PZT film has a rhombohedral crystal structure. No significant change in peak position is observed up to 5 at % Ce addition, whereas in the 10 at % Ce-doped sample the broad hump around $2\theta = 28.7^\circ$ is due to CeO_2 precipitation. This is clearer in the slow-scanned X-ray diffractogram (Fig. 3 inset).

The lattice parameters for different compositions are given in Table II. For undoped PZT the measured values of a_R and α_R are 0.408 nm and 90.06° respectively. These compare well with the values reported in the literature [24]. No appreciable change in lattice parameters with composition is found (Table II) and the small changes are within experimental error. Kala [25] also found that the rhombohedral phase parameter did not change with Zr/Ti ratio.

4.2. Surface morphology

The SEM micrographs and grain size distribution of the samples are shown in Figs 4 and 5, respectively. In the undoped film the grain boundaries are clearly visible (Fig. 4a), but for the 0.05 and 0.1 at % Ce-doped films the grain boundaries are relatively blurred. In the PZT films PbO is the only volatile species which can evaporate during the annealing treatment. The blurred nature of the grain boundaries in 0.05 and 0.1 at % Ce-doped samples probably indicates that the Pb loss has reduced in these samples.

There is a distinct increase in grain size upon initial addition of CeO_2 up to 1 at % (Fig. 4a–d and Fig. 5.) However further additions of CeO_2 result in a very significant decrease in grain size. Voids and craters within the grains are clearly visible in 1, 3 and 5 at % CeO_2-doped samples. The large grains in 1 at % samples are cracked. Apparently the addition of CeO_2 increases the grain boundary mobility leading to grain growth and trapping of porosity within the grains. The cracks nucleate from these pores in large grains due to the thermal stresses produced during cooling.

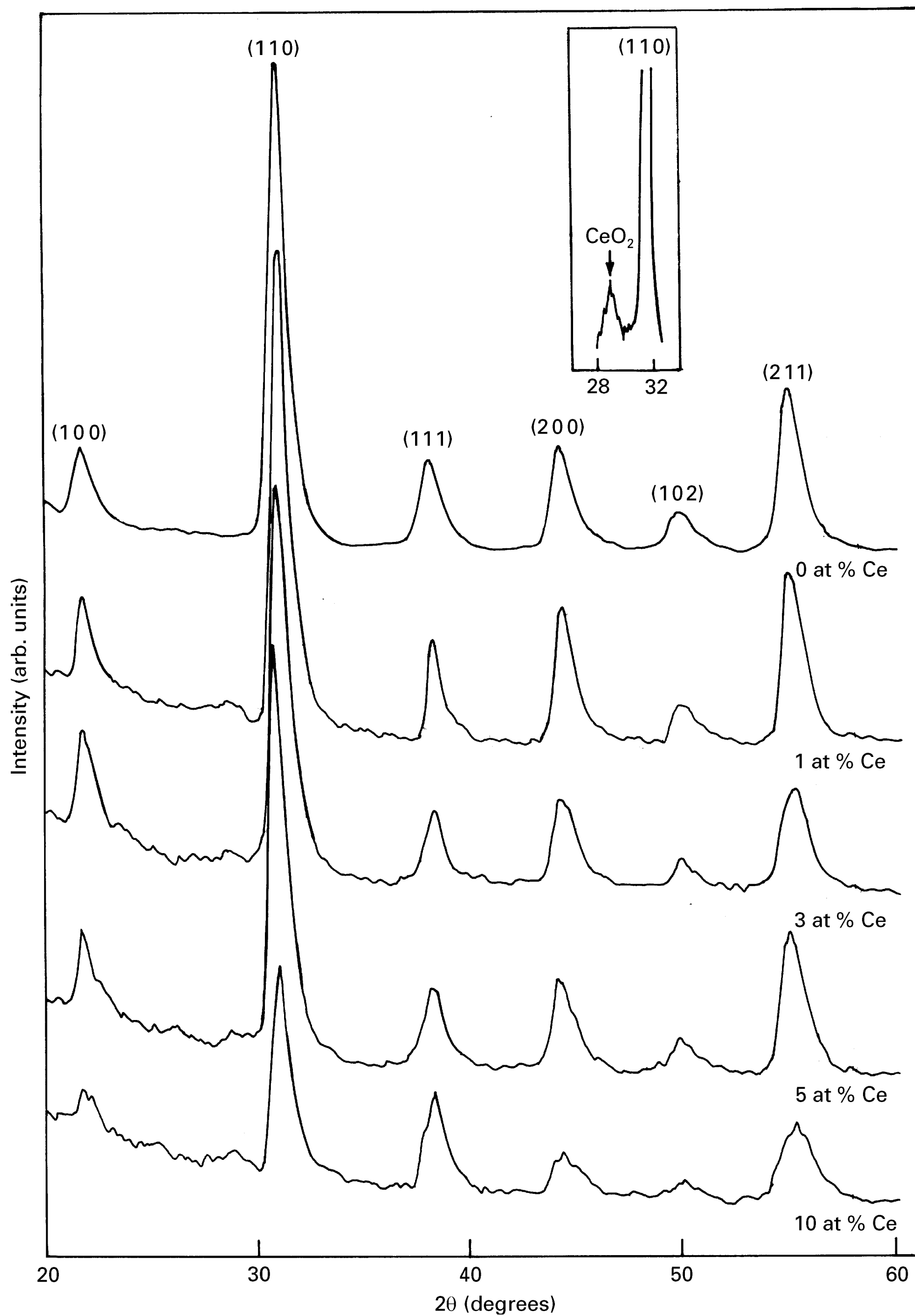

Figure 3 X-ray diffractograms of pure and cerium doped PZT films; inset shows CeO_2 precipitation at 10 at % Ce doping.

TABLE II Lattice parameters of Ce-doped PZT film

% CeO_2	2θ	d_{hkl}	(hkl)	Phase	Lattice parameter (a_R) (nm)	Angular distortion (α_R) (°)
0	44.35	2.040	200	Rhombohedral	0.408	90.05
	49.95	1.824	102			
1.0	44.4	2.038	200	Rhombohedral	0.407	89.53
	49.8	1.829	102			
3.0	44.35	2.040	200	Rhombohedral	0.408	89.77
	49.85	1.827	102			
5.0	44.3	2.040	200	Rhombohedral	0.408	89.80
	49.8	1.829	102			

Further addition of CeO_2 inhibits grain growth, perhaps due to the presence of precipitated CeO_2 which is not detectable by X-rays except at the highest CeO_2 concentration (10 at %).

4.3. Evaluation of the optical constants

Fig. 2 shows the typical transmission spectra of the weakly absorbing PZT film on a completely transparent sapphire $(1\,1\,\bar{2}\,0)$ substrate. The interference fringes

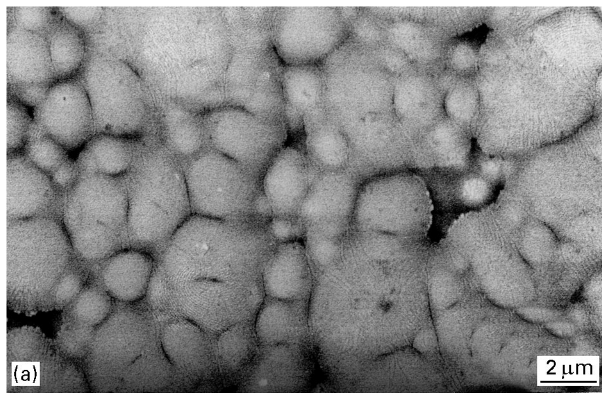

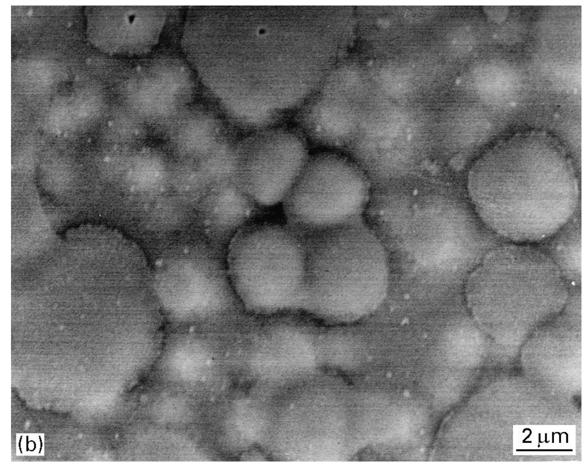

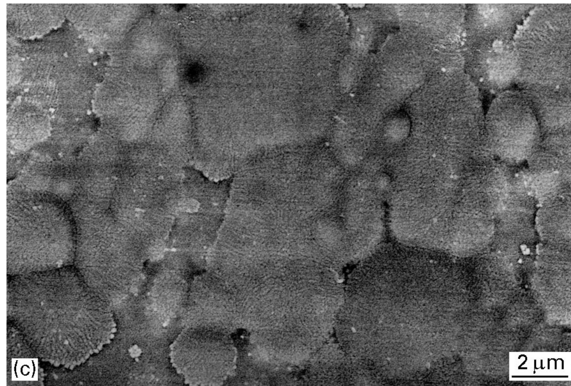

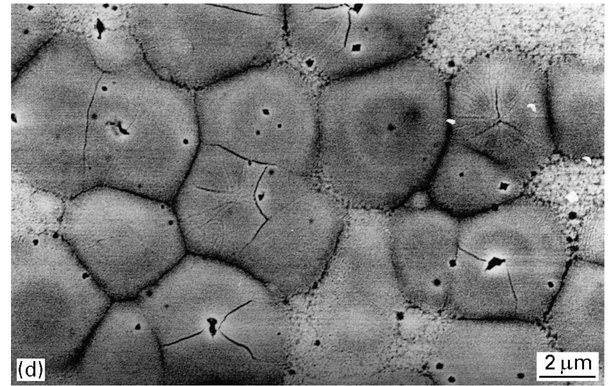

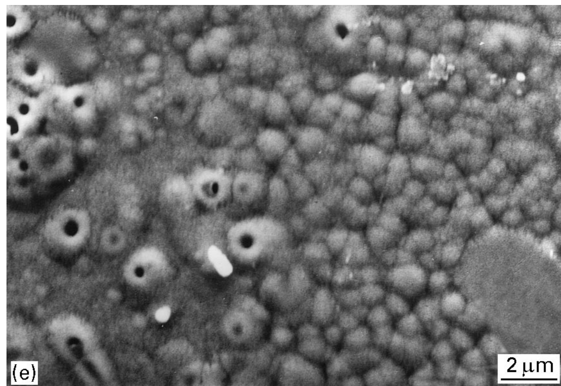

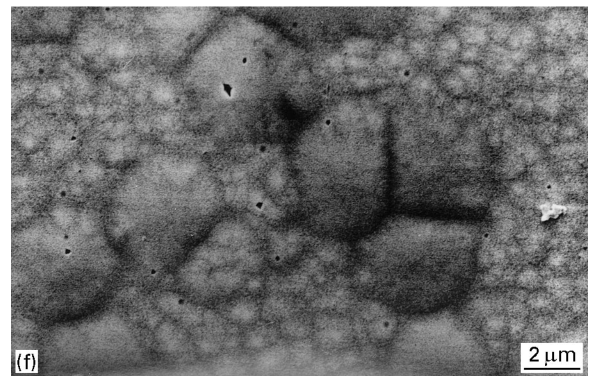

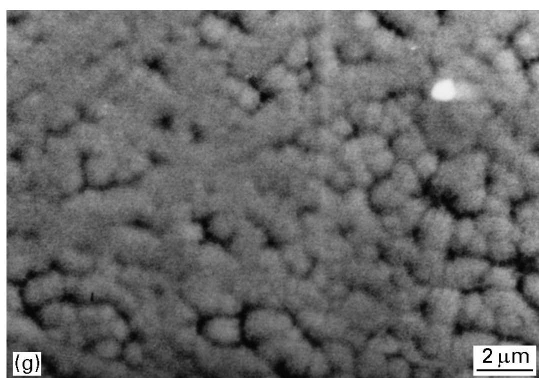

Figure 4 SEM micrographs of undoped and cerium doped PZT thin films on sapphire: (a) undoped, (b) 0.05 at % Ce, (c) 0.1 at % Ce, (d) 1 at %, Ce, (e) 3 at % Ce, (f) 5 at % Ce and (g) 10 at % Ce.

are a result of the interference between two interfaces: the air–film and film–substrate. Even slight variation in the thickness of the film will destroy the fringe pattern. In the present set of experiments for almost all the samples (except 1 at % Ce-doped film), well resolved fringe patterns have been obtained. It indicates that there is little variation of thickness in the annealed film [26]. As expected, the maxima of the interference fringes in the reflection spectra are the minima in the transmission spectra and vice versa.

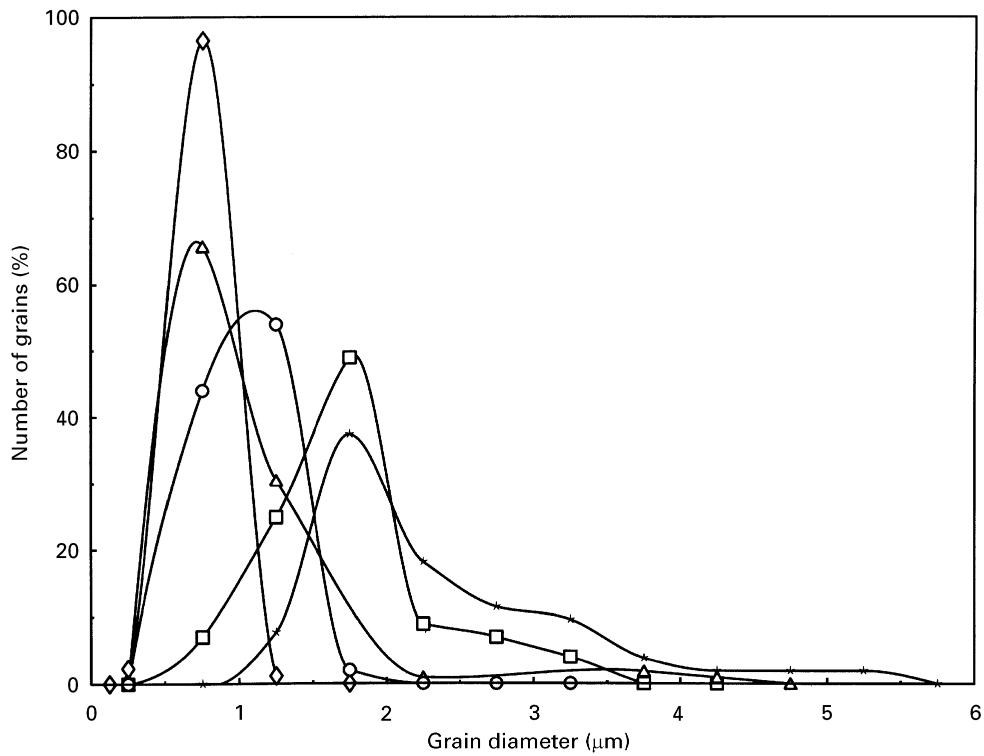

Figure 5 Grain size distribution of PZT and Ce-doped PZT thin films (Key: □ 0 at % Ce; ☆ 1 at % Ce; ◇ 3 at % Ce; △ 5 at % Ce; ○ 10 at % Ce).

The transmission spectra can be sub-divided into three distinct regions: weak absorption region ($T > 0.6$), medium absorption region ($0.6 \geqslant T \geqslant 0.4$) and strong absorption region ($T \leqslant 0.4$). The weak and medium absorption range of the spectra have been used to determine refractive index (n) as a function of wavelength (λ) using the "envelope method" described earlier. In the weak absorption region the transmittance $T(\lambda)$ of the sample has been enveloped by two dashed curves T_{max} and T_{min} as shown in Fig. 2 and the refractive index of the film as a function of λ calculated using Equation 7, as described earlier.

Fig. 6 shows the plot of refractive index (n) as a function of photon wavelength (λ) for the undoped PZT film. At He–Ne laser wavelength of $\lambda = 632.8$ nm, it is seen that the refractive index value of the undoped PZT is lower than the corresponding bulk and thin film refractive index values which are 2.55 [23] and 2.32 [10], respectively. The lower n value obtained could be due to the porosity

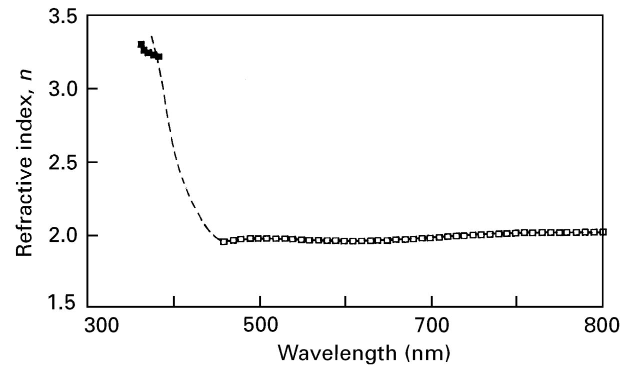

Figure 6 Refractive index as a function of wavelength for undoped film (□ transmittance measurement; ■ reflectance measurement).

and/or stresses in the films [10]. Table III summarizes the value of the optical constants obtained from the present study. The slight increase of n with Ce doping is attributed to improved densification

TABLE III Summary of the optical results

Composition at % Ce (100δ)	Thickness (nm)		Refractive, index, n	Extinction coefficient, k	Packing fraction, f	Band gap, E_g(eV)
	Optically determined	Surface profilometer	(at 632.8 nm)			
0	1765	1750	1.94	0.002	0.623	3.39
0.05	1055	1000	2.00	0.005	0.663	3.33
0.1	853	850	2.01	0.007	0.666	3.25
1.0	–	1000	–	–	–	3.31
3.0	808	790	2.02	0.003	0.671	3.48
5.0	1228	1200	2.14	0.009	0.743	3.16
10.0	792	800	2.15	0.007	0.747	3.25

TABLE IV Calculation of the thickness of undoped PZT film

Composition	λ	n	d' (nm)	$\bar{d}'$ (nm)	m'	m	d (nm)	$\bar{d}$ (nm)	$\bar{d}$ S.P.
O–Ce PZT	773.58 (p)	1.98	1745.83		8.76	9	1761		
	686.79 (p)	1.95	1787.04		9.74	10	1765		
	620.75 (p)	1.94		1713.8	10.70	11	1762	1765	1750
	834.61 (v)	1.98	1553.77		8.15	8.5	1788		
	728.30 (v)	1.97	1817.92		9.25	9.5	1760		
	652.83 (v)	1.94	1664.73		10.19	10.5	1765		
	592.45 (v)	1.94			11.22	11.5	1756		

NB p = peak position, v = valley position, S.P. = measured by surface profilometer.

of PZT with Ce addition or change in Zr/Ti ratio [10].

The function $(n^2 - 1)^{-1}$ was plotted against λ^{-2} in accordance with the single-term Sellmeier dispersion formula for one dominant electronic oscillator as described in Section 3.1. For undoped PZT film the typical values of S_0, λ_0 and refractive index dispersion parameter, $hc/e\lambda_0 S_0$ (where h, c and e are the Planck's constant, velocity of light and electronic charge), were 0.26×10^{15} m^{-2}, 0.13 μm and 3.81×10^{-14} eV m^2, respectively. The value of S_0, λ_0 obtained are low as compared to the reported values of sputter deposited perovskite PZT films [27]; this could probably arise from the different processing routes, lower density or stress in our films. On the other hand, the refractive index dispersion parameter compares well with that of the model of Di Domenico and Wemple [19] which states that its value should be smaller than $(6 \pm 0.6) \times 10^{-14}$ eV m^2 owing to the contribution of Pb^{2+} in PZT solid solutions.

The very occurrence of interference fringes points to the homogeneity of thickness in the films. The thickness can be calculated with precision as described earlier if the refractive index corresponding to adjacent maxima or minima is known. Table IV shows an example of such a calculation for undoped PZT film. The accuracy in thickness values is significantly increased by this procedure. Thus in Table IV the standard deviation for d' is 94.12 nm whereas that for d is 9.95 nm. Although the films were prepared using an identical number of coating cycles, the range of thickness of final annealed film varies from 793 to 1765 nm. Not all sols were prepared at the same time, and since there is a gradual rise in sol viscosity with time during storage, this leads to this variation in thickness.

The thickness values were used to calculate the extinction coefficients (k) as a function of λ for all the films. Fig. 7 shows the plot of k as a function of λ for undoped PZT. The extinction coefficients of cerium-doped PZT thin films in the visible and infrared regions were in the order of 10^{-3} which is comparable to reported values for metalorganic chemical vapour deposition (MOCVD) PZT films [10] indicating good surface homogeneity of the films studied.

Since the envelope method is not valid in the strong absorption region, the calculation of the absorption coefficients of the film needs both the transmission and reflection spectra. Equation 12 has been used to calculate the absorption coefficient (α) as a function of photon energy ($h\nu$). Fig. 8 shows the plot of α^2 versus $h\nu$. Assuming direct band transition we have calculated the band gap (E_g) of all the films. Table III and Fig. 9 show the variation of optical band energy (E_g) of the films with % Ce doping. There is a significant and sharp drop in E_g upon initial doping up to 0.1 at % CeO_2. E_g then increases and reaches a peak at 3 at % CeO_2 before decreasing and nearly levelling off

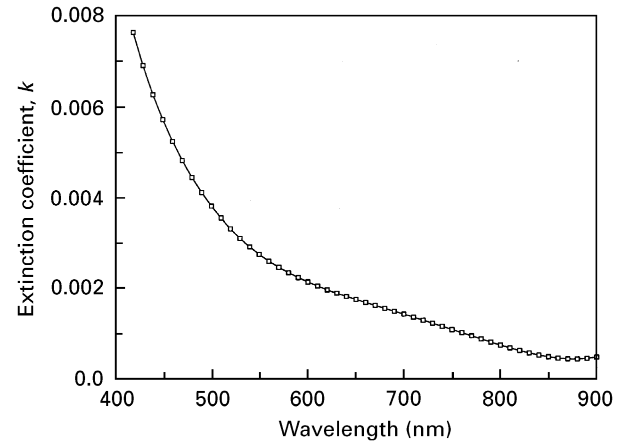

Figure 7 Extinction coefficient as a function of wavelength for undoped film.

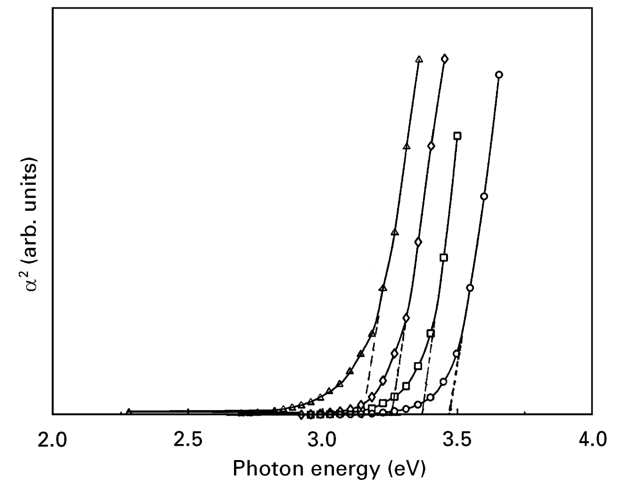

Figure 8 Square of absorption coefficient as a function of photon energy for undoped (□), 0.1 (◇), 3 (○) and 5 at % (△) Ce-doped PZT thin films.

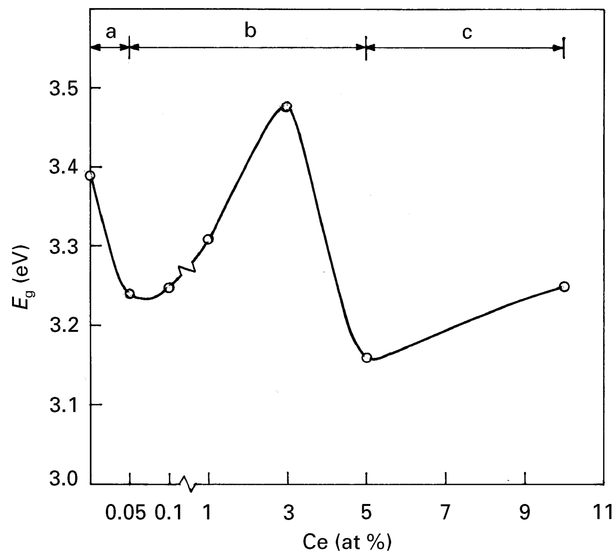

Figure 9 Variation of band gap energy (E_g) with Ce addition.

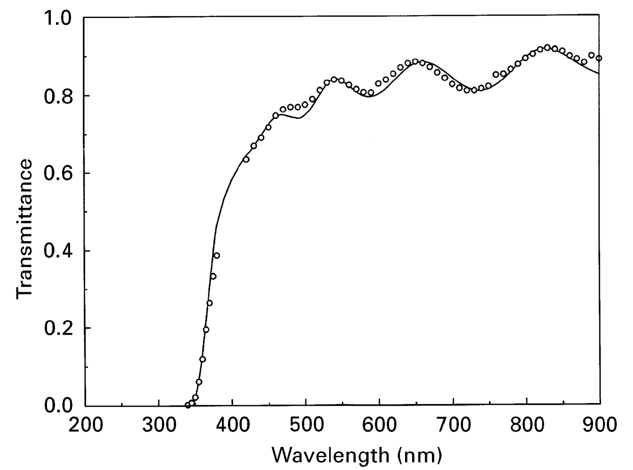

Figure 10 Comparison of the calculated transmission spectrum (—) with the experimental spectrum (○) for the 3 at % Ce-doped PZT film.

between 5 to 10 at % CeO_2. The observed variations are significant and the magnitude of the changes are much larger than the experimental uncertainties.

Rajopadhye *et al.* [28] reported that in the case of Nb-, Sr- and La-doped $Pb_{0.95}D_{0.05}(Zr_{0.53}Ti_{0.47})O_3$ film where D denotes the dopant concentration, there is no change in the absorption edge position, indicating that the band gap in PZT does not change due to the addition of dopants. On the other hand, Sreenivas *et al.* [29] have reported that the optical absorption edge is a very strong function of film composition. They reported the absorption edge for pure PZT at 340 nm. However the as-deposited film had an absorption edge at 380 nm (when the substrate temperature was 25 °C) or 360 nm (when substrate temperature was 200 °C). Okada [30] reported an absorption edge change from 330 nm in the pyrochlore phase to 295 nm in the perovskite phase for r.f. diode sputtered films. Krupanidhi *et al.* [31] reported a similar change occurring from 430 to 350 nm in r.f. magnetron sputtered films. It was concluded that the incorporation of excess PbO into the perovskite phase during film growth or loss of PbO due to evaporation results in the observed shift from the higher wavelength (more free PbO) to the lower wavelength (single perovskite phase film or lead deficient film) [31]. In the present case there is no systematic variation in E_g with % CeO_2 which shows that there must exist competing factors controlling the absorption edge and thereby the band gap value. An attempt is made in the following to correlate these factors with the changes in E_g. Region a in Fig. 9 corresponds to the first addition of CeO_2 to PZT. Even though while preparing the film it is assumed that Ce goes to B(Zr) sites, it is quite posssible that at least some of the Ce may go to A(Pb) sites. This would result in the creation of A site vacancies to balance the charge. Also the introduction of Ce in the lattice would result in some strain. One or both of these factors may be responsible for the observed sharp drop in E_g up to 0.1 at % CeO_2.

Between 0.1 and 3 at % CeO_2 (region b in Fig. 9) E_g gradually increases and peaks at 3 at % CeO_2. The stresses in the lattice in this composition range are likely to be relieved due to void and crack formation in the film (Fig. 4d–e). Also there may be a change in the relative occupancy of A and B sites by Ce. These factors may be responsible for the observed increase in E_g. Between 3 and 10 at % CeO_2, the grain size of the film is reduced drastically and there is precipitation of free CeO_2. This is accompanied by a decrease and levelling off in the value of E_g. These results demonstrate that optical properties are quite sensitive to processing conditions and microstructure of the film.

The packing fraction (f) of each film was calculated using the effective medium approximation (EMA). Table III summarizes these results. The packing fraction shows a slight increase with Ce doping from 0.62 (undoped) to 0.75 (10 at % Ce doped film). This indicates the improved densification of the film with Ce doping. It should be noted that since the bulk n value (at $\lambda = 632.8$ nm) for undoped PZT, corresponding to morphotropic phase boundary composition (Zr/Ti = 0.53/0.47), is not known, in calculating f we have used an interpolated n value as suggested in the literature [10] for all the compositions in this present study. It could lead to a lower calculated f value.

As a demonstration of the validity of our procedures and consistency of values of optical constants derived from it, we use them to fit the transmission spectra of which a typical plot is shown in Fig. 10. The excellent fit obtained requires only less than 1% change in the d value and reproduces all features of the experimentally obtained spectra.

5. Conclusions

Transparent cerium-doped PZT thin films (0.7–1.7 μm thick) have been prepared on single-crystalline sapphire ($11\bar{2}0$) substrates. X-ray analysis reveals that the films have a predominantly perovskite rhombohedral structure. Up to 5 at % Ce no phase separation is detectable, however, at 10 at % Ce doping, CeO_2 precipitates out. Addition of a small quantity of Ce^{4+} into the PZT lattice probably inhibits the PbO loss. Addition of more than 1 at % Ce^{4+} reduces the

average grain size of the films. The refractive indices of the film are low compared to the bulk material. This is attributed to the porosity in the films. The low values of the extinction coefficients indicate excellent surface homogeneity of the films. The thickness values obtained from optical measurement compare well with the surface profilometer data. There is some improvement in the packing fraction with cerium doping. Significant change in the band gap energy values with Ce^{4+} addition have been obtained. Several factors including Pb loss, induced lattice strain due to cerium inclusion or change in Zr/Ti ratio in the films, could have influenced this change. Further study is required to identify the exact contribution of each of the above factors.

References

1. B. JAFFE, "Piezoelectric Ceramics" (Academic Press Inc, New York, 1971).
2. TAKAHASHI MIHARA, HITOSHI WATANABE and C. A. PAZ DE ARAUJO, *Jpn J. Appl Phys.* **32** (1993) 4168.
3. K. SREENIVAS, M. SAYER, D. J. BAAR and M. NISHIOKA, *Appl. Phys. Lett* **52** (1988) 709.
4. K. IIJIMA, Y. TOMITA, R. TAKAYAMA and I. UEDA, *J. Appl. Phys.* **60** (1986) 361.
5. H. ADACHI, T. MITSUYU, O. YAMAZAKI and K. WASA, *ibid.* **60** (1986) 736.
6. S. B. MAJUMDER, D. C. AGRAWAL, Y. N. MOHAPATRA and V. N. KULKARNI, *Integrated Ferroelectrics* **9** (1995) 271.
7. S. B. MAJUMDER, V. N. KULKARNI, Y. N. MOHAPATRA and D. C. AGRAWAL, *Bull. Mater. Sci.* **22** (1994) 1005.
8. A. H. CARIM, B. A. TUTTLE, D. H. DOUGHTY and S. L. MARTINEZ, *J. Amer. Ceram. Soc.* **74** (1991) 1455.
9. KAZUSHI AMANUMA, TORU MORI, TAKASHI HASE, TOSHIYUKI SAKUMA, ATSUSHI OCHI and YOICHI MIYASAKA, *Jpn J. Appl. Phys.* **32** (1993) 4150.
10. CHIEN H. PENG and SESHU B. DESU, *J. Amer. Ceram. Soc.* **77** (1994) 929.
11. JOON SUNG LEE, CHANG JUNG KIM, DAE SUNG YOON, CHAUN GI CHOI, JAE MYUNG KIM and KWANGSOO NO, *Jpn J. Appl. Phys.* **33** (1994) 260.
12. RYOICHI TAKAYAMA, YOSHIHIRO TOMITA, KENJI IIJIMA and ICHIRO UEDA, *J. Appl. Phy.* **63** (1988) 5868.
13. D. F. RYDER Jr and N. K. RAMAN. *J. Electron. Mater.* **21** (1992) 971.
14. A. H. CARIM, *J. Amer. Ceram. Soc.* **74** (1991) 1455.
15. P. DURAN, M. GONZALEZ, C. MOURE, J. JURADO and C. PASCUAL, *J. Mater. Sci.* **24** (1990) 5001.
16. B. D. CULLITY, "Elements of X-ray Diffraction" (Addision Wesley Publishing Company, Inc., California, 1978).
17. J. C. MANIFACIER, J. GASIOT and J. P. FILLARD, *J. Phys E: Sci. Instrum.* **9** (1976) 1002.
18. I. H. MALITSON, *J. Opt. Soc. Amer.* **52** (1967) 1377.
19. M. DI DOMENICO, Jr, S. H. WEMPLE, *J. Appl. Phys* **40** (1969) 720.
20. A. J. DEKKER, "Solid State Physics" (MacMillan India Limited, India, 1985).
21. R. H. BUBE, "Electronic Properties of Crystalline Solids" (Academic, New York, 1974) Ch. 11.
22. D. A. G. BRUGGEMAN, *Ann. Phys* (*Leipzig*) **24** (1935) 636.
23. P. D. THATCHER, *Appl. Opt.* **16** (1977) 3210.
24. GUANGHUA YI, ZHENG WU and M. SAYER, *J. Appl. Phys.* **64** (1988) 2717.
25. T. KALA, *Phys. Status Solidi* (*a*) **78** (1983) 277.
26. R. SWANEPOEL, *J. Phys. E: Sci. Instrum.* **9** (1976) 1002.
27. J. KREMPASKY, L. WANG, M. PROCTOR, A. PIGNOLET and F. LEVY, *Solid State Comm.* **78** (1991) 1039.
28. N. R. RAJOPADHYE, S. V. BHORASKAR, S. BADRINARAYAN and A. P. B. SINHA, *J. Mater. Sci.* **23** (1988) 2631.
29. K. SREENIVAS, M. SAYER and P. GARRETT, *Thin Solid Films* **172** (1989) 251.
30. A. OKADA, *J. Appl. Phys.* **48** (1977) 2905.
31. S. B. KRUPANIDHI, N. MAFFEI, M. SAYER and K. EL ASSAL, *ibid.* **54** (1983) 6601.

Received 10 October 1995
and accepted 19 November 1996.